Analysis of 14q12 microdeletions reveals novel regulatory loci for the neurodevelopmental disorder-related gene, *FOXG1*

Aishwarya Ramamurthy[1], Masha D Bandouil[1], Likhita Aluru[1], Ojasi Joshi[1], Esther Yoon[1], Nicholas Bodkin[1], Jennifer Z Cheng[1], Carina G Biar[1], Jeffrey D Calhoun[1], Gemma L Carvill[1,2] *

Affiliations:

1. Ken and Ruth Davee Department of Neurology, Northwestern University Feinberg School of Medicine, Chicago, IL, USA
2. Department of Pharmacology, Northwestern University Feinberg School of Medicine, Chicago, IL, USA

Abstract (149/150 words)

Up to 17% of neurodevelopmental disorders (NDDs) can be explained by pathogenic structural variants (SVs) that disrupt coding regions and elicit gene dosage defects. However, noncoding SVs which can perturb *cis*-regulatory elements (CREs) and downstream gene expression are understudied. In this study, we describe multiple 14q12 deletions downstream of NDD-related gene *FOXG1* in individuals with overlapping phenotypes of *FOXG1* haploinsufficiency. We show that deletion of a minimum region of overlap (MRO) reduced *FOXG1* expression, disrupted CREs and altered *FOXG1*'s native genomic interactions. Deleting the MRO did not fully eliminate *FOXG1* expression, indicating that multiple CREs likely cooperate to regulate *FOXG1* and would need to be deleted to completely prevent expression. The transcriptomic profiles of MRO loss overlap in part with *FOXG1* loss, including direct FOXG1 targets, indicating converging molecular pathways. These findings expand the scope of *FOXG1's* complex regulatory region, and more broadly, of regulatory SVs in NDD susceptibility.

Introduction

Neurodevelopmental disorders (NDDs) are a heterogenous collection of developmental disorders that impair functions of the brain and the nervous system. These disorders have childhood onset and include, among others, intellectual disability (ID), autism spectrum disorder (ASD) and epilepsy. It is now well established that disease-causing protein-coding variants in hundreds of genes account for up to 40% of NDDs [1,2]. This still leaves a large fraction of cases unexplained, rekindling interest in investigating the noncoding regulatory regions of the genome for causative variants in individuals with NDDs.

In particular, structural variants (SVs) are attractive candidates for understanding noncoding variation due to the thousands to millions of base pairs that can be disrupted and thus, in theory, easier interpretation as compared to single nucleotide variants (SNVs). SVs, defined as alterations greater than 50 base pairs, include deletions, duplications, insertions, inversions, and translocations. SVs can overlap known NDD-related genes and cause these conditions through gene dosage effects. Coding SVs account for 15-17% of NDDs in general [3,4] and 10-12% of specific NDDs, such as the genetic epilepsies [5–7]. However, some SVs do not span coding regions but rather disrupt cis-regulatory elements (CREs) or higher order chromatin structures, including topologically associated domains (TADs). When SVs disrupt CREs, promoter-enhancer interactions can be perturbed, which affects gene transcription [8–10]. For example, noncoding SNVs and duplications in the *GATA2* regulatory region cause hereditary congenital facial paresis [11]. These variants cause disease by aberrant prolonged *GATA2* expression which in turn impairs an essential neural fate switch during development [11]. SVs can also disrupt TAD boundaries, leading to an alteration of the native chromatin architecture, promoting non-canonical promoter-enhancer interactions and gene misexpression. TAD disruption by SVs has been reported in human limb malformations and congenital disorders [12,13]. Moreover, noncoding variants in the TAD encompassing NDD-related gene, *MEF2C* were present in excess in a large genomic screen of individuals with NDDs, and deletion of a proximal *MEF2C* TAD boundary resulted in reduced gene expression [14,15]. Collectively, these studies highlight an emerging role for noncoding SVs in the etiology of NDDs. Here we add to this burgeoning field by describing NDD-related microdeletions at the 14q12 locus flanking the gene, *FOXG1*.

FOXG1 encodes Forkhead Box G1, a key transcription factor in forebrain development that is highly dosage sensitive [16]. *FOXG1* expression is especially critical during corticogenesis, triencephalon specification and development, as well as maintenance of mature neurons [17,18]. Neurodevelopment is reliant not only on precise spatio-temporal *FOXG1* expression, but also on its cellular expression levels; both increased and decreased *FOXG1* expression is associated with poor neurological outcomes [16,19,20]. Heterozygous loss of *FOXG1* causes *FOXG1* syndrome, a congenital NDD characterized by epilepsy, ID, microcephaly, developmental delays, loss of motor skills and overlapping clinical features with Rett syndrome [21–23]. Several heterozygous *de novo* whole gene deletions, truncating variants and loss of function missense variants cause *FOXG1* syndrome. The pathogenic mechanism is thus haploinsufficiency, wherein one autosomal allele of *FOXG1* is functional, but insufficient to prevent disease

[22]. In addition, *de novo* duplications of *FOXG1* result in increased gene dosage and are associated with developmental epilepsy, ID, and severe speech impairment [24].

SVs overlapping putative CREs have also been described in individuals with overlapping clinical features of *FOXG1* haploinsufficiency, but without coding variants [23,25–27]. While the impact of these deletions on *FOXG1* expression was examined, results have been contradictory, likely owing to the virtually absent *FOXG1* expression in accessible peripheral patient biospecimens (Supplementary Fig. 1). Specifically, one group showed increased *FOXG1* in blood and saliva from individuals with 14q12 deletions and predicted a single region of overlap (SRO) to be regulatory [25]. Conversely, another showed reduced *FOXG1* expression in blood, despite shared regions of overlap across patient-specific deletions (Fig. 1) [26]. To address these inconsistencies, here we refined the SRO to a new minimum region of overlap (MRO) in individuals with *FOXG1* haploinsufficient clinical features and downstream deletions, and modeled the MRO in the HAP1 cell line which robustly expresses *FOXG1*. We refine the regulatory landscape of the *FOXG1* locus and demonstrate that MRO deletion reduced *FOXG1* expression, likely contributing to haploinsufficiency in individuals with NDDs.

Results

Deletion of downstream *FOXG1* 14q12 minimum region of overlap leads to reduced *FOXG1* expression

We identified 9 microdeletions in the 14q12 region downstream of *FOXG1* described in DECIPHER. These deletions were reported in individuals (6 females and 3 males) with ID (n=8), seizures (n=3) and microcephaly (n=6) (Fig. 1 and Table 1). Most of these deletions were *de novo* (patients 2-7); one deletion was maternally inherited (patient 9) and two were of unknown inheritance (patient 1 and 8). None of these deletions encompassed any other gene except *PRKD1. PRKD1* is tolerant to loss of function in the general population with a pLI score of 0 and LOEUF of 0.76 (gnomAD, [28,29]), has very low expression in the brain compared to other tissues (GTEx), and the mouse knockout has no neurological phenotype (MGI:99879), collectively suggesting *PRKD1* loss is not associated with NDDs. Thus, we hypothesized that disruption of CREs in the region likely contributed to the phenotype via disruption of *FOXG1* expression. We selected the minimum region of overlap (MRO) between these deletions for modeling in the HAP1 cell line. This region (hg38: chr14:29,704,736-29,803,897) spans ~0.1 Mb and is ~0.93 Mb downstream of *FOXG1*. The MRO was examined for variants in the general population using gnomAD and no large deletions were observed in this locus (Supplementary Fig. 2).

We selected the HAP1 cell line due to its haploid nature, which facilitates genome editing, as well as the endogenous expression of *FOXG1* (Supplementary Fig. 1 and Fig. 2). We successfully deleted the MRO using dual flanking guides in HAP1s (14q12-MRO-Del); the entire *FOXG1* coding region was similarly deleted as a positive control ($FOXG1^{KO}$). We verified the genotypes of 14q12-MRO-Del (deletion of hg38: chr14:29,704,715-29,803,900) and $FOXG1^{KO}$ (deletion of hg38: chr14:28,767,269-28,768,758) using Sanger sequencing, and in the 14q12-MRO-Del confirmed the absence of major off-target SVs using genome sequencing (Supplementary Fig. 3). We

121 confirmed the loss of *PRKD1* exon 2 and flanking intronic sequence at both the genomic
122 DNA and mRNA level in 14q12-MRO-Del (Supplementary Fig. 3-4).

123 Using qRT-PCR, we demonstrated complete loss of *FOXG1* mRNA expression in
124 $FOXG1^{KO}$ and a 61% reduction in the 14q12-MRO-Del line (p-value 0.0006, Welch's T
125 test) (Fig. 2A). At the protein level, western blotting revealed similar loss of protein in
126 $FOXG1^{KO}$ and a 45% reduction in the 14q12-MRO-Del (p-value 0.0005, Welch's T test)
127 (Fig. 2B). Collectively, these results demonstrate that deleting the MRO reduces
128 *FOXG1* expression, though not to the same degree as deletion of the complete coding
129 region.

130 Deletion of the MRO locus alters *FOXG1's* native contacts with downstream CREs

131 To examine the causal mechanism of reduced *FOXG1* expression with MRO deletion,
132 we examined chromatin interactions of the *FOXG1* locus with downstream CREs in
133 wildtype and 14q12-MRO-Del lines using Unique Molecular Identifier (UMI)-4C. We
134 anchored the viewpoint proximal to *FOXG1's* promoter (Supplementary Table 4) and
135 identified 9997 UMIs in WT and 6805 UMIs in 14q12-MRO-Del. UMI-4C contact
136 intensity profiles were generated which highlight multiple promoter – CRE interactions
137 across the 14q12 region (Fig. 3). The overwhelming majority of contacts lie downstream
138 of *FOXG1*, with very few contacts, and no peaks upstream. The CRE landscape across
139 this region is complex with many known and predicted regulatory regions and most
140 have high levels of conservation (Fig. 3). This includes nine VISTA enhancers active in
141 neurodevelopment, of which six show forebrain-specific activity (Hs1064, Hs566,
142 Hs1523, Hs342, Hs433, Hs344) (Supplementary Fig. 5) [30,31]. In addition, there is an
143 enhancer cluster near Hs598, with five active forebrain-specific enhancers in a zebrafish
144 model [32]. A massively parallel reporter assay (MPRA) in fetal brain and cerebral
145 organoids further reveals dozens of active CREs [33]. As well as these demonstrated
146 active CREs, in both HAP1s and neural cell lineages there are a number of putative
147 enhancers, defined by the histone modification, H3K27Ac [30,31,34–37]. Deleting the MRO
148 not only led to loss of UMI-4C contacts in this region as expected, but also altered
149 native *FOXG1* genomic interactions. Specifically, significant differences in UMI contacts
150 between WT and 14q12-MRO-Del were observed at six 14q12 loci, including four
151 regions with increased contacts and two that were decreased (Fig. 3, Supplementary
152 Fig. 6). Of note, four of these enhanced contacts (3 increased, one decreased) were
153 located 1.5 Mb downstream of *FOXG1*, extending beyond a TAD boundary present in
154 HAP1s, embryonic stem cells (ESCs), neural progenitor cells (NPCs) and neurons (Fig.
155 3). These contacts suggest that *FOXG1* regulation extends beyond this TAD boundary,
156 substantiated by the presence of inter boundary looping interactions as well
157 (Supplementary Fig. 7-8).

158 As expected, in the 14q12-MRO-Del, physical genomic interactions were lost between
159 the *FOXG1* promoter and the MRO locus (Fig. 3 and Fig. 4A). Deletion of the 14q12-
160 MRO results in the deletion of at least two, but possibly more enhancers, as defined by
161 H3K27Ac peaks in the HAP1 cell line (Fig. 4A). We selected these two H3K27Ac peaks
162 (cCRE1 and cCRE2) in the MRO to test for enhancer activity in the HAP1 cell line and
163 the HT-22 cell line derived from mouse hippocampus. cCRE1, which has high levels of
164 conservation, showed a statistically significant 1.6-fold and 3.4-fold increase in

expression in HAP1s and HT-22s, respectively (Fig. 4B). Conversely, cCRE2 reduced expression of the reporter by 2.5 - 4.8-fold in each cell type. Due to size constraints, we could not test both cCREs simultaneously, which would be more reflective of the context specific regulatory potential of the MRO. Nevertheless, in this system, our data suggests that both cCRE1 and cCRE2 have regulatory potential, and deletion of at least the cCRE1 element could underpin the reduced *FOXG1* expression elicited by MRO deletion. Given that both the cCRE H3K27Ac peaks are present in stem cell derived neural precursor lines and the human brain (Fig. 4A), and that there are two additional active regulatory elements (Fig. 4A - MPRA active 1/2,[33]) in the developing human brain within the MRO, we collectively conclude that the MRO locus is likely regulatory in a neuronal context and MRO loss results in reduced *FOXG1* expression.

<u>Gene expression analysis identifies shared DEGs between 14q12-MRO-Del and *FOXG1*^{KO}</u>

Given *FOXG1's* role as a transcription factor, we evaluated the effects of *FOXG1* downregulation on overall gene expression changes using RNA-seq. We identified 1036 differentially expressed genes (DEGs) in 14q12-MRO-Del, and 517 DEGs in FOXG1^{KO}, compared to WT. *FOXG1* was a DEG in both lines with a larger effect in FOXG1^{KO} (log2FC -2.753916 and adjusted p-value 8.484237e-34), as compared to the 14q12-MRO-Del line (log2FC -0.7397485 and adjusted p-value 0.002290243). Furthermore, we identified 86 DEGs that overlapped between the two datasets. The shared DEGs included genes involved in cell cycle regulation (*CCND1, BMP7)* [38–40] as well as those implicated in epilepsy (*FOSL2, ELAVL3, EPHA5*, *OLFM3, ARHGAP4)* [41–45], ID/microcephaly (*XYLT1, COLEC11, CADPS2)* [46–48], and other NDDs (*KY, ADGRL3, TCEAL9)* [49–51] (Fig. 5 and Supplementary Data 1). Functional enrichment analysis of DEGs revealed a few shared molecular functions and biological pathways between 14q12-MRO-Del and FOXG1^{KO} including terms relevant in a neuronal context: "regulation of nervous system development", "axon/neuron projection guidance" and "regulation of neurotransmitter levels" (Supplementary Fig. 9). We also used two existing chromatin immunoprecipitation sequencing experiments from mouse embryonic brain (E15.5 cortex [52] and E16.5 ganglionic eminence [53]) to identify 8007 genes bound by Foxg1. Of these direct Foxg1 targets, a comparable fraction were also DEGs in the FOXG1^{KO} and 14q12-MRO-Del lines (17% (86/517 DEGs) in FOXG1^{KO} and 15% (154/1036 DEGs) in 14q12-MRO-Del) (Supplementary Data 1). These results are comparable to the 33% of DEGs that are direct targets of Foxg1 in the mouse ganglionic eminence [53]. Thus collectively, even though we modeled MRO loss in a non-neuronal HAP1 cell line, we observe overlapping DEGs, including direct Foxg1 targets, in the MRO deletion and *FOXG1* coding loss, suggesting shared downstream effects of reduced expression of this transcription factor.

Discussion

FOXG1 is a dosage sensitive gene where both over and under expression are associated with epilepsy and NDDs [16,54,55]. SVs, especially microdeletions in the 14q12 region downstream of *FOXG1* are reported in several individuals with clinical phenotypes that resemble *FOXG1* haploinsufficiency [23,25–27]. Whether the observed phenotypes are a result of the deletions remains unclear, and the complex mechanisms

of *FOXG1* regulation by CREs in this region, and how the microdeletions might disrupt this landscape are not fully understood. We identified nine 14q12 microdeletions downstream of *FOXG1* in DECIPHER in individuals with epilepsy, ID and/or microcephaly, and having no other clear causal variants. The deletions ranged from ~151.8 kb to 1.17 Mb in size and were of mostly unspecified pathogenicity. We identified a shared 0.1 Mb region (MRO), deleted in all patients, nearly 0.93 Mb distal to *FOXG1* that regulates *FOXG1* expression.

Deletion of the MRO led to reduced *FOXG1* expression by roughly half in the HAP1 cell line, possibly due to the deletion of cCRE1 which activated expression of a reporter gene in HAP1s. This cCRE is highly conserved across evolution and correlates with a peak of H3K27Ac in HAP1s and a distal enhancer signature in ENCODE, collectively suggesting it functions as an enhancer in HAP1s. However, the second H3K27Ac peak, cCRE2 which is poorly conserved, reduced expression of the reporter gene in HAP1s and shows correlation with H3K4me3 and DNAse hypersensitivity from ENCODE CREs usually demarcating promoter regions. Taken together, the impact of cCRE2 is less clear; while there is good evidence that cCRE1 deletion may reduce expression of *FOXG1* in HAP1s. Further, cCRE1 increased expression of a reporter gene to an even greater extent in a mouse hippocampal cell line and also shows some evidence of H3K27Ac enrichment in a neuronal context. Moreover, there are two additional active enhancers in the MRO detected from primary cortical fetal brain tissue [33]. Collectively, our data in HAP1s and HT-22s, as well as our reanalysis of published data, suggests that the MRO has the potential to regulate *FOXG1* expression, and that deletion of this region leads to reduced FOXG1 and contributes to the development of neurological features in individuals with 14q12 deletions.

Deletion of the MRO reduced *FOXG1* expression but did not eliminate it, indicating that multiple CREs across the region need to be deleted to abrogate *FOXG1* expression. Indeed, the MRO lies within a larger regulatory region of *FOXG1* designated as the SRO (smallest region of overlap); previously defined by *de novo* 14q12 deletions downstream of *FOXG1* in three individuals with *FOXG1* syndrome related phenotypes including epilepsy, ID, developmental delays and severe postnatal microcephaly . The SRO is a complex region with multiple validated, highly conserved active enhancers in mouse, zebrafish and human fetal brain tissue and organoid models [30–33]. We refined the SRO to the MRO based on the distal deletions in patient 8 and 9. Of note, these two individuals present with ID only. In contrast, individuals with deletion of both the SRO and MRO (patient 1-7) generally present with more severe clinical features of *FOXG1* haploinsufficiency: ID, seizures and microcephaly (**Table 1**). These varied clinical presentations, taken together with the reduction, but not complete loss of *FOXG1* by MRO deletion, suggests that disruption of multiple CREs is required to completely ablate *FOXG1* expression. Moreover, the number of disrupted CREs may underpin genotype-phenotype relationships; where individuals with deletion of more CREs have lower *FOXG1* expression and clinical features more reminiscent of individuals with *FOXG1* coding variants, while individuals with fewer CREs deleted (e.g. patients 8 and 9) have less severe clinical presentation correlated with higher FOXG1 abundance. Indeed, this modulated view of *FOXG1* expression finds support in other neurological conditions. For instance, there are multiple GWAS loci in the 14q12 regulatory region

254 that have been associated with increased risk for ADHD and schizophrenia [56]. Deletion
255 of a ~500 bp region flanking a schizophrenia-associated SNP rs1191551 reduced
256 *FOXG1* expression by ~20% in HEK293T cells [57]. Moreover, a luciferase assay
257 demonstrated reduced activity of the risk rs1191551 allele, suggesting that even this
258 single nucleotide change can modulate *FOXG1* expression. Collectively, these studies
259 highlight the need to systematically assess both disease-associated SVs and single
260 nucleotide changes across this regulatory region in neurological disease broadly, and
261 that variable gene expression across neurodevelopment may have varied phenotypic
262 consequences. As genome sequencing facilitates more widespread and smaller SV and
263 SNV detection, these genotype-phenotype relationships may become more apparent.

264 In addition to the loss of contacts in the MRO, we also observed increased distal
265 contacts beyond a putative TAD boundary in the 14q12-MRO-Del HAP1 line. This
266 included three increased contacts with regions that harbor forebrain-specific, active
267 VISTA enhancers, and are supported by contact maps in human NPCs and neurons as
268 well. These results support the notion of enhancer redundancy across the 14q12 locus.
269 Tight regulation via multiple CREs is a known characteristic of developmental genes,
270 particularly those that are exquisitely sensitive to dosage during mammalian
271 development [58]. This redundancy is likely a protective mechanism against deleterious
272 genomic aberrations [59]. For instance, individual deletion of each of ten regulatory
273 elements involved in mouse limb development resulted in normal limb phenotypes,
274 whereas pairwise deletions of these loci resulted in noticeably different limb formations,
275 demonstrating partial redundancy [59]. These redundant, or shadow enhancers regulate
276 the same target gene and overlap in part or full, in the developmental space and time to
277 fine tune gene dosage [58]. Similarly, *FOXG1* expression is subject to tight spatiotemporal
278 regulation during corticogenesis. Furthermore, the effect of shadow enhancers on gene
279 expression is not always additive; depending on the availability of transcription factors at
280 each of the enhancers and the buffering requirement of the cell, the effects can be
281 superadditive, subadditive, or even repressive [58,60]. Here we demonstrate that there are
282 multiple CREs within the MRO that may regulate *FOXG1* expression, but that there are
283 likely additional redundant enhancers across the 14q12 locus region. Testing this
284 hypothesis, however, is challenging, and a limitation of the dual sgRNA guide genome-
285 editing strategy used in this study to introduce the ~100 kb MRO deletion. While newer
286 methods such as dCas9-controlled CRISPR/Cas3 can generate deletions on a
287 megabase scale [61], our approach has too low an efficiency to introduce the >400 kb
288 SRO. Future studies, using Cas3-like deletion approaches in cellular and animal models
289 are key for examining the redundancy of CREs in the 14q12 region, and the absolute
290 number of CREs that need to be deleted to abrogate *FOXG1* expression. Furthermore,
291 massively parallel reporter assays (MPRA) in human neurodevelopmental stem cell
292 models and human tissues, such as those described [33], are likely to be essential for
293 assessing the activity of individual CREs.

294 We examined the transcriptional profile of the MRO deletion and FOXG1 knockout lines,
295 demonstrating overlap in the genes that were differentially expressed, notably BMP
296 family protein *BMP7* [40], *CCND1*, a G1 phase cyclin [39] and *EGR1*, a transcription factor
297 and member of the EGR-*FOXG1* coupled regulatory network [62]. Of note, these genes
298 have overlap with the known roles of FOXG1 in a neuronal context, including

modulating BMP signaling and the cell cycle, ensuring cells remain in proliferative states [19,40]. As well as these single genes, key biological pathways of neurodevelopment were also enriched for DEGs, including overlapping genes in both models of *FOXG1* reduction. While these results are encouraging, they do highlight a limitation of our study, in that we do not demonstrate the impact of MRO loss in a neuronal cell line. We selected HAP1s because of the ease of editing and robust FOXG1 abundance, and are confident that at least some of the regulatory landscape is overlapping, but we acknowledge that this is not a neuronal line. We did also generate iPSC lines heterozygous for MRO deletion and differentiated them to neural cell types. However, we found inconsistent *FOXG1* expression in iPSC-derived NPCs and iPSC-derived neurons that was not reproducible, even in wildtype control lines (data not shown). High variability in the endogenous expression of this gene is also seen in previous iPSC studies [20,40]. Therefore, collectively we could not use these neuronal models as an effective experimental system to study the effects of MRO- and *FOXG1* loss. In the future, reporter-based systems, and live-imaging will be necessary to accurately quantify the temporal expression of FOXG1 in iPSC-derived models, to counteract the variability inherent in these systems.

In summary, our work refines the regulatory landscape of the *FOXG1* locus, and we identify a ~0.1 Mb regulatory region downstream of *FOXG1* in the 14q12 region. Within this MRO, we define putative *FOXG1* CREs and emphasize that this locus exhibits both enhancer redundancy as well as shadow enhancer activity. The complex regulatory nature of the *FOXG1* locus is reflected in its importance in disease etiology. We define the causal mechanisms of a subset of clinical features of *FOXG1* syndrome and posit that deletion of multiple CREs is necessary to cause *FOXG1* haploinsufficiency. Overall, this critical regulatory locus should be examined across both NDDs and neuropsychiatric disease for causative and contributory variants, presenting unique opportunities for gene-targeting therapies via modulation of *FOXG1* expression.

Methods

Cell line maintenance

Human eHAP (fully haploid engineered HAP1) cells from Horizon Discovery BioSciences (C669) were maintained in IMDM (Thermo Fisher Scientific) supplemented with 10% Tet-approved FBS (Atlanta Biologicals) and 1% penicillin/streptomycin (Thermo Fisher Scientific). Mouse hippocampal HT-22 cells (Sigma SCC129) were maintained in DMEM containing 4.5 g/l glucose (Thermo Fisher Scientific) supplemented with 10% Tet-approved FBS (Atlanta Biologicals) and 1% penicillin/streptomycin (Thermo Fisher Scientific). The cells were tested for mycoplasma contamination, and all experiments were performed within 3 to 10 passages.

Selection of candidate 14q12 microdeletions and cell line generation

We used DECIPHER (DatabasE of genomiC varIation and Phenotype in Humans using Ensembl Resources) [63] to identify 14q12 microdeletions downstream of the NDD-related gene, *FOXG1* in individuals with epilepsy and related NDDs. Deletions within *FOXG1's*

342 TAD that excluded *FOXG1* and extended up to hg38: chr14:30,550,000 (approaching
343 the distal TAD boundary limit) were considered [64]. Larger deletions spanning multiple
344 genes were excluded as gene dosage effects from multiple encompassed genes are
345 likely to confound patient phenotypes.

346 CRISPR genome editing was used to create 14q12-MRO-Del and FOXG1^{KO} HAP1
347 lines. Guide RNAs were designed to target each of the two breakpoints of the MRO and
348 cloned into a Cas9-GFP vector (PX458, Addgene #48138) or a Cas9-mCherry vector (a
349 PX458 derivative engineered in-house) (Supplementary Table 1 for guide RNA
350 sequences). Dual guide electroporation was performed using the Neon Transfection
351 System. 24-48h post transfection, FACS was performed for single cell clonal isolation
352 and expansion of GFP and mCherry double positive cells. Clonal lines were genotyped
353 by PCR, followed by Sanger sequencing, to detect the presence of the deletion
354 (Supplementary Table 1 for primer sequences). Whole genome sequencing (WGS) was
355 performed to further confirm the intended genotype. Moreover, we used the MetaSV
356 pipeline to detect the presence of any large unintended SVs, and any lines harboring
357 such variants were excluded [65]. FOXG1^{KO} lines were similarly generated, with dual
358 guide RNAs targeting the start and end of *FOXG1*'s coding region (Supplementary
359 Table 1). Clones of 14q12-MRO-Del and FOXG1^{KO}, along with the parental/unedited
360 line (WT Clone A) and a wildtype clone from the CRISPR screen (WT Clone B) as
361 isogenic controls, were selected for experimentation (Supplementary Table 2).
362

363 <u>*FOXG1* mRNA and protein quantification</u>

364 Quantitative reverse transcription PCR was performed to assay *FOXG1* mRNA levels.
365 RNA was extracted and purified from HAP1s in culture using TRIzol reagent
366 (Invitrogen #15596026). qRT-PCR reactions were performed using Biorad iTaq
367 Universal One-Step RT-qPCR Kit (1725150). 25ng RNA per reaction was used and
368 triplicate qRT-PCR reactions were carried out for each target (Supplementary Table 1)
369 on a Biorad CFX384 Real-Time PCR Detection system. Raw Ct values were obtained
370 for each sample. Ct values for *FOXG1* were transformed by first normalizing to EAR
371 and then normalizing to WT to calculate relative fold change of *FOXG1* [66]. Two Sample
372 T-Test (Welch's T-Test) was performed to test statistical significance between samples.
373 *PRKD1* mRNA quantification was similarly performed.
374
375 Western blotting was performed to assay FOXG1 protein levels. Whole cell lysates were
376 prepared using RIPA Lysis and Extraction Reagent (Thermo Scientific 89900) in the
377 presence of protease inhibitors (cOmplete™, Mini, EDTA-free Protease Inhibitor
378 Cocktail, Sigma 11836170001). 20 µg of protein per well was separated on NuPage 3-
379 8% Tris-Acetate precast gels (Invitrogen) and transferred onto a PVDF membrane
380 (Millipore). Immunoblotting was performed using primary antibodies (Supplementary
381 Table 3) and detected with peroxidase-conjugated secondary antibodies
382 (Supplementary Table 3). This was followed by detection with ECL peroxidase substrate
383 (Cytiva Amersham RPN2232). Protein band intensities on immunoblots were quantified
384 by densitometric analysis. Two Sample T-Test (Welch's T-Test) was performed to test
385 statistical significance between samples.

386 Locus specific chromatin capture

387 UMI-4C was performed for targeted and quantitative capture of *FOXG1*'s genomic
388 interactions with the following specifications [14]. *FOXG1* viewpoint was defined as a 1 kb
389 window at the 5' end of the gene. Crosslinked chromatin from 5 x 10^6 cells were used
390 per sample. UMI-4C libraries were constructed by enriching the 4C library for *FOXG1*
391 contacts using viewpoint specific primers (Supplementary Table 1) [32]. Two unique
392 barcode adapters per sample were utilized to generate five UMI-4C reactions per
393 adapter, which were pooled to make a final UMI-4C library. UMI-4C experiments were
394 performed at least twice per clone. Libraries were subject to 75 bp paired end
395 sequencing on the Illumina MiniSeq platform at a sequencing depth of 1-2M reads per
396 sample.

397 Raw read quality was assessed using FastQC [67]. The fastq files from sequencing were
398 analyzed using the UMI-4C R Package as described [14,68]. Since the UMI-4C library is
399 made up of adapter ligated DNA fragments that consist of both the bait and its spatially
400 proximal genomic region, it generates sequencing reads that map to both these loci. To
401 quantify these spatially proximal genomic interactions, the R package transforms the
402 raw sequencing reads to unique genomic interactions (UMI counts) per genomic
403 restriction fragment and the resulting data is saved as genomic tracks. From these
404 tracks, we extracted viewpoint-specific UMI counts for a given region of interest using
405 the package. UMI counts were normalized to the total UMI counts within the region of
406 interest and a smoothed interaction profile was produced using default parameters in
407 the package. In this way, we generated UMI-4C profiles for the 14q12 region of interest
408 (hg38: chr14: 28,965,045-30,631,045) for WT and 14q12-MRO-Del samples. Differential
409 genomic interactions between samples were evaluated using the UMI4Cats R package
410 [69]. Significant differential contacts between WT and 14q12-MRO-Del were inferred by
411 the Wald Test using the waldUMI4C() function with FDR adjusted *p*-value of 0.05.

412 Analysis of H3K27Ac data across 14q12 *FOXG1* regulatory region

413 H3K27Ac ChIP-seq data was assessed from published data in HAP1s (GSE167721),
414 adult brain hippocampus (GSM1112791) and temporal lobe (GSM772995), the
415 embryonic stem cell line H1 (GSM466732) as well as neural precursor cells (NPCs)
416 derived from H1 (GSM753429) and ganglionic eminence neurospheres derived from H1
417 (GSM1127083).

418 Validation of MRO cCREs using luciferase assay

419 The regulatory activity of cCREs was evaluated in HAP1 and HT-22 cell lines using the
420 Dual-Luciferase® Reporter Assay System (Promega E1910). cCRE sequences
421 (Supplementary Table 5) were cloned into the pGL4.23[luc2/minP] vector (Promega
422 E8411) containing firefly luciferase. The pGL4.74[hRluc2TK] Vector (Promega E6921)
423 with *Renilla* luciferase was used as internal transfection control. pGL4.23 minus an
424 upstream cCRE sequence (Empty) was used as control for baseline firefly luciferase
425 expression. Dual transfection of pGL4.23 and pGL4.74 plasmids was performed using
426 Xfect (Takara Bio) for HAP1s, and Lipofectamine (Thermo Fisher Scientific) for HT-22s.
427 Cells were assayed 48h post transfection. Luminescence from Firefly luciferase was
428 first normalized to the internal *Renilla* luciferase control and then further normalized to

the Empty control to calculate relative fold change of luciferase reporter expression with cCREs. Experiments were repeated four times.

Bulk RNA-Seq library prep and data analysis

RNA was extracted and purified from HAP1s in culture by the guanidinium thiocyanate-phenol-chloroform extraction method using TRIzol™ reagent (Invitrogen #15596-026). Purified RNA samples were assayed on a TapeStation 4150 (Agilent) to determine the concentration and RIN (RNA Integrity Number) values. RNA samples with RIN > 9 were sent to Novogene for mRNA library preparation and subject to 150 bp paired end sequencing on a NovaSeq platform at a sequencing depth of at least 20 M reads per sample.

Raw read quality was assessed using FastQC [67]. Reads were trimmed to remove adapter sequences using HTStream, aligned to the human reference genome GRCh38/hg38 and GENCODE v38 using STAR [70]. The read count matrix was generated using GENCODE v38 using Rsubread [71]. Differentially expressed genes (DEGs) were detected using DESeq2 using an adjusted p-value threshold of 0.05 and log2Fold change greater/less than absolute value of 1 [72]. Functional enrichment analysis was performed using gene ontology in the clusterProfiler package using a Benjamini-Hochberg corrected p-value threshold of 0.05 [73–76]. Published FOXG1 peaks were retrieved from prior work [52,53] and the overlapping (i.e. present in either dataset) set of genes (n=8007) were used to identify the direct FOXG1 genes that were also DEGs.

Reporting summary

Further information on research design is available in the Nature Research Reporting Summary linked to this article.

Data availability

The main data supporting the findings of this study are available within the article and its Supplementary Information. Source data are provided with this paper. UMI-4C and RNA-Seq raw data files from this study are available at the NCBI SRA database with BioProject accession number PRJNA1348521. Additional details on datasets and protocols of this study will be made available by the corresponding author upon reasonable request.

Author contributions: AR, MB, LA, OJ, EY, JZC and CB generated the experimental data. NB and JDC assisted with experiments. AR, JDC, GLC performed data analysis and interpretation of results. GLC and AR conceived the presented idea, developed the theory, wrote this manuscript and generated figures for this manuscript. GLC supervised the project.

Acknowledgements: Our work was supported by the following funding sources: the Chicago Biomedical Consortium Catalyst Award to GLC and the American Epilepsy Society Predoctoral Fellowship to AR.

Competing interests: All authors declare no competing interests.

476 **References**

477 1. McRae, J. F. *et al.* Prevalence and architecture of de novo mutations in
478 developmental disorders. *Nature 2017 542:7642* 542, 433–438 (2017).

479 2. Jansen, S., Vissers, L. E. L. M. & de Vries, B. B. A. The Genetics of Intellectual
480 Disability. *Brain Sciences 2023, Vol. 13, Page 231* 13, 231 (2023).

481 3. Kaminsky, E. B. *et al.* An evidence-based approach to establish the functional and
482 clinical significance of copy number variants in intellectual and developmental
483 disabilities. *Genet Med* 13, 777–784 (2011).

484 4. D'haene, E. & Vergult, S. Interpreting the impact of noncoding structural variation
485 in neurodevelopmental disorders. *Genetics in Medicine* 23, 34–46 (2021).

486 5. Hebbar, M. & Mefford, H. C. Recent advances in epilepsy genomics and genetic
487 testing. *F1000Res* 9, (2020).

488 6. Helbig, K. L. *et al.* Diagnostic exome sequencing provides a molecular diagnosis
489 for a significant proportion of patients with epilepsy. *Genet Med* 18, 898–905
490 (2016).

491 7. Retterer, K. *et al.* Clinical application of whole-exome sequencing across clinical
492 indications. *Genet Med* 18, 696–704 (2016).

493 8. Cauwelier, B. *et al.* Molecular cytogenetic study of 126 unselected T-ALL cases
494 reveals high incidence of TCRβ locus rearrangements and putative new T-cell
495 oncogenes. *Leukemia 2006 20:7* 20, 1238–1244 (2006).

496 9. Weischenfeldt, J. *et al.* Pan-cancer analysis of somatic copy-number alterations
497 implicates IRS4 and IGF2 in enhancer hijacking. *Nature Genetics 2016 49:1* 49,
498 65–74 (2016).

499 10. Wang, X. *et al.* Genome-wide detection of enhancer-hijacking events from
500 chromatin interaction data in rearranged genomes. *Nature Methods 2021 18:6* 18,
501 661–668 (2021).

502 11. Tenney, A. P. *et al.* Noncoding variants alter GATA2 expression in rhombomere 4
503 motor neurons and cause dominant hereditary congenital facial paresis. *Nature*
504 *Genetics 2023 55:7* 55, 1149–1163 (2023).

505 12. Ibn-Salem, J. *et al.* Deletions of chromosomal regulatory boundaries are
506 associated with congenital disease. *Genome Biol* 15, 423 (2014).

507 13. Lupiáñez, D. G. *et al.* Disruptions of Topological Chromatin Domains Cause
508 Pathogenic Rewiring of Gene-Enhancer Interactions. *Cell* 161, 1012–1025 (2015).

509 14. Mohajeri, K. *et al.* Transcriptional and functional consequences of alterations to
510 MEF2C and its topological organization in neuronal models. *Am J Hum Genet*
511 109, 2049–2067 (2022).

512 15. Redin, C. *et al.* The genomic landscape of balanced cytogenetic abnormalities
513 associated with human congenital anomalies. *Nat Genet* 49, 36–45 (2017).

514 16. Hettige, N. C. & Ernst, C. FOXG1 Dose in Brain Development. *Front Pediatr* 7,
515 482 (2019).

516 17. Xuan, S. *et al.* Winged helix transcription factor BF-1 is essential for the
517 development of the cerebral hemispheres. *Neuron* 14, 1141–1152 (1995).

518 18. Dastidar, S. G., Landrieu, P. M. Z. & D'Mello, S. R. FoxG1 Promotes the Survival
519 of Postmitotic Neurons. *Journal of Neuroscience* 31, 402–413 (2011).

520 19. Hanashima, C., Shen, L., Li, S. C. & Lai, E. Brain Factor-1 Controls the
521 Proliferation and Differentiation of Neocortical Progenitor Cells through
522 Independent Mechanisms. *Journal of Neuroscience* 22, 6526–6536 (2002).

523 20. Hettige, N. C. *et al.* FOXG1 dose tunes cell proliferation dynamics in human
524 forebrain progenitor cells. *Stem Cell Reports* 17, 475–488 (2022).

525 21. Ariani, F. *et al.* FOXG1 Is Responsible for the Congenital Variant of Rett
526 Syndrome. *The American Journal of Human Genetics* 83, 89–93 (2008).

527 22. Mitter, D. *et al.* FOXG1 syndrome: genotype–phenotype association in 83 patients
528 with FOXG1 variants. *Genetics in Medicine 2018 20:1* 20, 98–108 (2017).

529 23. Kortüm, F. *et al.* The core FOXG1 syndrome phenotype consists of postnatal
530 microcephaly, severe mental retardation, absent language, dyskinesia, and
531 corpus callosum hypogenesis. *J Med Genet* 48, 396–406 (2011).

532 24. Brunetti-Pierri, N. *et al.* Duplications of FOXG1 in 14q12 are associated with
533 developmental epilepsy, mental retardation, and severe speech impairment.
534 *European Journal of Human Genetics 2011 19:1* 19, 102–107 (2010).

535 25. Allou, L. *et al.* 14q12 and severe Rett-like phenotypes: new clinical insights and
536 physical mapping of FOXG1-regulatory elements. *Eur J Hum Genet* 20, 1216–
537 1223 (2012).

538 26. Ellaway, C. J. *et al.* 14q12 microdeletions excluding FOXG1 give rise to a
539 congenital variant Rett syndrome-like phenotype. *European Journal of Human*
540 *Genetics 2013 21:5* 21, 522–527 (2012).

541 27. Mehrjouy, M. M. *et al.* Regulatory variants of FOXG1 in the context of its
542 topological domain organisation. *European Journal of Human Genetics 2017 26:2*
543 26, 186–196 (2017).

544 28. Karczewski, K. J. *et al.* The mutational constraint spectrum quantified from
545 variation in 141,456 humans. *Nature 2020 581:7809* 581, 434–443 (2020).

546 29. Rausell, A. *et al.* Common homozygosity for predicted loss-of-function variants
547 reveals both redundant and advantageous effects of dispensable human genes.
548 *Proc Natl Acad Sci U S A* 117, 13626–13636 (2020).

549 30. Visel, A., Minovitsky, S., Dubchak, I. & Pennacchio, L. A. VISTA Enhancer
550 Browser--a database of tissue-specific human enhancers. *Nucleic Acids Res* 35,
551 (2007).

552 31. Kosicki, M. *et al.* VISTA Enhancer browser: an updated database of tissue-
553 specific developmental enhancers. *Nucleic Acids Res* 53, (2025).

554 32. Hamerlinck, L. *et al.* Non-coding structural variants identify a commonly affected
555 regulatory region steering FOXG1 transcription in early neurodevelopment.
556 *medRxiv* 2025.03.10.25323301 (2025) doi:10.1101/2025.03.10.25323301.

557 33. Deng, C. *et al.* Massively parallel characterization of regulatory elements in the
558 developing human cortex. *Science (1979)* 384, 868–876 (2024).

559 34. Dunham, I. *et al.* An integrated encyclopedia of DNA elements in the human
560 genome. *Nature* 489, 57–74 (2012).

561 35. Abascal, F. *et al.* Expanded encyclopaedias of DNA elements in the human and
562 mouse genomes. *Nature 2020 583:7818* 583, 699–710 (2020).

563 36. Hitz, B. C. *et al.* The ENCODE Uniform Analysis Pipelines. *bioRxiv*
564 https://doi.org/10.1101/2023.04.04.535623 (2023)
565 doi:10.1101/2023.04.04.535623.

566 37. Luo, Y. *et al.* New developments on the Encyclopedia of DNA Elements
567 (ENCODE) data portal. *Nucleic Acids Res* 48, D882–D889 (2020).

568 38. Pedraza, N. *et al.* Cytoplasmic expression of the cell cycle regulator cyclin D1 in
569 radial glial progenitor cells modulates brain cortex development. *bioRxiv*
570 2024.12.23.630056 (2024) doi:10.1101/2024.12.23.630056.

571 39. Lottini, G. *et al.* Zika virus induces FOXG1 nuclear displacement and
572 downregulation in human neural progenitors. *Stem Cell Reports* 17, 1683 (2022).

573 40. Hettige, N. C. *et al.* FOXG1 targets BMP repressors and cell cycle inhibitors in
574 human neural progenitor cells. *Hum Mol Genet* 32, 2511 (2023).

575 41. Cospain, A. *et al.* FOSL2 truncating variants in the last exon cause a
576 neurodevelopmental disorder with scalp and enamel defects. *Genetics in*
577 *Medicine* 24, 2475–2486 (2022).

578 42. Wutikeli, H., Xie, T., Xiong, W. & Shen, Y. ELAV/Hu RNA-binding protein family:
579 key regulators in neurological disorders, cancer, and other diseases. *RNA Biol* 22,
580 1–11 (2025).

43. Liu, T. T. *et al.* [Changes in the expression of EphA5/ephrinA5 in the CA3 region of the hippocampus in rats with epilepsy and their role in the pathogenesis of temporal lobe epilepsy]. *Zhongguo Dang Dai Er Ke Za Zhi* 19, 1272–1277 (2017).

44. Tang, S. *et al.* Olfactomedin-3 Enhances Seizure Activity by Interacting With AMPA Receptors in Epilepsy Models. *Front Cell Dev Biol* 8, 557009 (2020).

45. Hu, Y. Y. *et al.* ARHGAP4 variants are associated with X-linked early-onset temporal lobe epilepsy. *World J Pediatr* 20, (2024).

46. LaCroix, A. J. *et al.* GGC Repeat Expansion and Exon 1 Methylation of XYLT1 Is a Common Pathogenic Variant in Baratela-Scott Syndrome. *Am J Hum Genet* 104, 35–44 (2019).

47. Gilissen, C. *et al.* Genome sequencing identifies major causes of severe intellectual disability. *Nature 2014 511:7509* 511, 344–347 (2014).

48. Bonora, E. *et al.* Maternally inherited genetic variants of CADPS2 are present in autism spectrum disorders and intellectual disability patients. *EMBO Mol Med* 6, 795–809 (2014).

49. Arif, B. *et al.* A novel homozygous KY variant causing a complex neurological disorder. *Eur J Med Genet* 63, 104031 (2020).

50. Menzel, M. H. M. M., Kohler, A., Hudemann, M., Jüngling, J. & Biskup, S. Case Report of a Juvenile Patient with Autism Spectrum Disorder with a Novel Combination of Copy Number Variants in ADGRL3 (LPHN3) and Two Pseudogenes. *Application of Clinical Genetics* 15, 125–131 (2022).

51. Albuainain, F. *et al.* Confirmation and expansion of the phenotype of the TCEAL1-related neurodevelopmental disorder. *European Journal of Human Genetics 2024 32:3* 32, 350–356 (2024).

52. Cargnin, F. *et al.* FOXG1 Orchestrates Neocortical Organization and Cortico-Cortical Connections. *Neuron* 100, 1083-1096.e5 (2018).

53. Sun, L. *et al.* Transcriptomic insights into fate choice of pallial versus subpallial GABAergic neurons. *Nat Commun* 16, (2025).

54. Li, J., Chang, H. . W., Lai, E., Parker, E. . J. & Vogt, P. . K. The oncogene qin codes for a transcriptional repressor - PubMed. *Cancer Res* 55, 5540–5544 (1995).

55. Seltzer, L. E. *et al.* Epilepsy and outcome in FOXG1-related disorders. *Epilepsia* 55, 1292–1300 (2014).

56. Cerezo, M. *et al.* The NHGRI-EBI GWAS Catalog: standards for reusability, sustainability and diversity. *Nucleic Acids Res* 53, D998–D1005 (2025).

57. Won, H. *et al.* Chromosome conformation elucidates regulatory relationships in developing human brain. *Nature* 538, 523 (2016).

58. Kvon, E. Z., Waymack, R., Gad, M. & Wunderlich, Z. Enhancer redundancy in development and disease. *Nature Reviews Genetics 2021 22:5* 22, 324–336 (2021).

59. Osterwalder, M. *et al.* Enhancer redundancy provides phenotypic robustness in mammalian development. *Nature 2018 554:7691* 554, 239–243 (2018).

60. Waymack, R., Fletcher, A., Enciso, G. & Wunderlich, Z. Shadow enhancers can suppress input transcription factor noise through distinct regulatory logic. *Elife* 9, 1–57 (2020).

61. Li, J. *et al.* Precise large-fragment deletions in mammalian cells and mice generated by dCas9-controlled CRISPR/Cas3. *Sci Adv* 10, 8052 (2024).

62. Hou, P. S., Miyoshi, G. & Hanashima, C. Sensory cortex wiring requires preselection of short- and long-range projection neurons through an Egr-Foxg1-COUP-TFI network. *Nature Communications 2019 10:1* 10, 1–18 (2019).

63. Firth, H. V. *et al.* DECIPHER: Database of Chromosomal Imbalance and Phenotype in Humans Using Ensembl Resources. *The American Journal of Human Genetics* 84, 524–533 (2009).

64. Wang, Y. *et al.* The 3D Genome Browser: A web-based browser for visualizing 3D genome organization and long-range chromatin interactions. *Genome Biol* 19, 1–12 (2018).

65. Mohiyuddin, M. *et al.* MetaSV: an accurate and integrative structural-variant caller for next generation sequencing. *Bioinformatics* 31, 2741–2744 (2015).

66. Livak, K. J. & Schmittgen, T. D. Analysis of relative gene expression data using real-time quantitative PCR and the 2(-Delta Delta C(T)) Method. *Methods* 25, 402–408 (2001).

67. Andrews, S. FastQC: A Quality Control Tool for High Throughput Sequence Data [Online]. Available online at: http://www.bioinformatics.babraham.ac.uk/projects/fastqc/. Preprint at https://doi.org/https://qubeshub.org/resources/fastqc (2010).

68. Schwartzman, O. *et al.* UMI-4C for quantitative and targeted chromosomal contact profiling. *Nat Methods* 13, 685–691 (2016).

69. Ramos-Rodríguez, M., Subirana-Granés, M. & Pasquali, L. UMI4Cats: an R package to analyze chromatin contact profiles obtained by UMI-4C. *Bioinformatics* 37, 4240–4242 (2021).

651 70. Dobin, A. & Gingeras, T. R. Mapping RNA-seq Reads with STAR. *Curr Protoc*
652 *Bioinformatics* 51, 11.14.1-11.14.19 (2015).

653 71. Liao, Y., Smyth, G. K. & Shi, W. The R package Rsubread is easier, faster,
654 cheaper and better for alignment and quantification of RNA sequencing reads.
655 *Nucleic Acids Res* 47, e47–e47 (2019).

656 72. Love, M. I., Huber, W. & Anders, S. Moderated estimation of fold change and
657 dispersion for RNA-seq data with DESeq2. *Genome Biol* 15, 550 (2014).

658 73. Yu, G., Wang, L. G., Han, Y. & He, Q. Y. ClusterProfiler: An R package for
659 comparing biological themes among gene clusters. *OMICS* 16, 284–287 (2012).

660 74. Wu, T. *et al.* clusterProfiler 4.0: A universal enrichment tool for interpreting omics
661 data. *The Innovation* 2, 100141 (2021).

662 75. Yu, G. Thirteen years of clusterProfiler. *The Innovation* 5, 100722 (2024).

663 76. Xu, S. *et al.* Using clusterProfiler to characterize multiomics data. *Nature*
664 *Protocols 2024 19:11* 19, 3292–3320 (2024).

665

666

667 **Table 1: Genetic and clinical details of 14q12 heterozygous deletion variants in individuals with epilepsy, ID**
668 **and/or microcephaly considered in defining the minimum region of overlap (MRO)**

Patient	Decipher ID	Sex	Deletion coordinates (hg38)	CREs deleted (Fig. 3)	Inheritance	Pathogenicity assignment in DECIPHER	Seizures	Intellectual Disability (ID)	Microcephaly	Additional clinical features
DECIPHER										
1	260836	46XY	14:29068799-29865858	6 VISTA enhancers, EC, HAP1-CRE1	Unknown	Unspecified	-	Yes	Yes	
2	248405	46XY	14:29226052-30403168	7 VISTA enhancers, EC, HAP1-CRE1	*De novo*	Unspecified	-	Yes	Yes	
3	3810	46XX	14:29226052-30403168	7 VISTA enhancers, EC, HAP1-CRE1	*De novo*	Unspecified	Yes	Yes	Yes	Bruxism, hypoplasia of the corpus callosum, delayed speech and language development
4	258584	46XX	14:29312198-30083730	3 VISTA enhancers, EC, HAP1-CRE1	*De novo*	Unspecified	Yes	Yes	-	Atypical behavior, delayed speech and language development
5	358785	46XX	14:29360119-29879052	3 VISTA enhancers, EC, HAP1-CRE1	*De novo*	Likely Pathogenic	-	Yes	Yes (secondary)	Agenesis of corpus callosum
6	414554	Female	14:29395780-29803897	1 VISTA enhancer, EC, HAP1-CRE1	*De novo*	Likely Pathogenic	Yes	-	Yes	Delayed myelination, global developmental delay, simplified gyral pattern
7	252353	46XX	14:29435514-29847454	1 VISTA enhancer, EC, HAP1-CRE1	*De novo*	Unspecified	-	Yes	Yes	Hypoplasia of the corpus callosum
8	259935	46XX	14:29704706-30500956	2 VISTA enhancers, HAP1-CRE1	Unknown	Unspecified	-	Yes	-	Atypical behavior
9 [27]	284715	46XY	14:29704736-29856618	HAP1-CRE1	Maternally inherited	Unspecified	-	Yes (mild)	-	Delayed speech and language development
Published (Ellaway *et al.*)[26]										
Case 1	-	Female	14:29226052-30403168	7 VISTA enhancers, EC, HAP1-CRE1	*De novo*	-	Yes	-	Yes	Intellectual impairment, agenesis of corpus callosum, global developmental delay
Case 2	-	Female	14:28868223-30018792	6 VISTA enhancers, EC, HAP1-CRE1	*De novo*	-	Yes	-	Yes	Intellectual impairment, agenesis of corpus callosum, global developmental delay
Case 3	-	Male	14:28960335-29847513	6 VISTA enhancers, EC, HAP1-CRE1	*De novo*	-	-	-	Yes	Intellectual impairment, severe developmental delay

669 Abbreviations: EC - Enhancer Cluster

670

671

672 Figure 1: 14q12 microdeletions downstream of *FOXG1* in this study. Deletions present
673 in individuals with epilepsy and other NDDs in DECIPHER are represented by horizontal
674 bars and color-coded for pathogenicity. Additionally, three deletions from prior work that
675 met our selection criteria are also shown (red horizontal bars) [26]. The overlap between
676 the 14q12 deletions was used to define the minimum region of overlap (MRO), in this
677 case by the deletion breakpoints in patients 6, 8 and 9 (black enclosure). The panel on
678 the right indicates whether individuals with the respective 14q12 deletions presented
679 with seizures, intellectual disability (ID) or developmental delays (DD) and microcephaly.
680 Grey bar represents a single overlapping region (SRO) in the 14q12 region previously
681 predicted to regulate *FOXG1* [25].
682
683 Figure 2: *FOXG1* expression is reduced with the loss of the MRO locus (A) *FOXG1*
684 mRNA fold change relative to *EAR* assayed by qRT-PCR (n: WT Clone A = 9, WT Clone
685 B = 3, 14q12-MRO-Del = 9, $FOXG1^{KO}$ = 3) (Two sample T-test, WT vs 14q12-MRO-Del,
686 p= 6.1e-4; WT vs $FOXG1^{KO}$, p = 4.5e-6). (B) FOXG1 protein levels relative to TAF5
687 were assayed using Western Blotting (n: WT Clone A =15, WT Clone B = 3, 14q12-
688 MRO-Del = 9, $FOXG1^{KO}$ = 6) (Two sample T-test, WT vs 14q12-MRO-Del, p= 5.1e-4;
689 WT vs $FOXG1^{KO}$, p = 4.7e-10). Error bars represent one standard error.

690 Figure 3: The *FOXG1* regulatory region is a complex landscape of multiple known and
691 putative CREs encompassing patient-specific deletions. The MRO defined by the 14q12
692 patient deletions in this study is highlighted in red. *FOXG1* UMI-4C profiles represent
693 genomic interactions of *FOXG1* in the 14q12 region (WT, grey; 14q12-MRO-Del;
694 purple). ADHD- and schizophrenia-associated GWAS loci [56], active CREs from MPRAs
695 in cerebral organoids and fetal brain samples [33], CREs defined by the enhancer histone
696 modification, H3K27Ac, as well as VISTA enhancers and ENCODE Candidate CREs
697 (cCREs) in this region overlap peaks from the UMI-4C contact profiles. Validated VISTA
698 enhancers that show enhancer activity in transgenic mice are shown in blue, and region
699 specificity shown in Supplementary Fig. 5 [30,31]. A previously described *FOXG1*
700 regulatory region, SRO (smallest region of overlap, horizontal grey bar) [25] in 14q12
701 encompasses VISTA enhancer hs598 with validated enhancer activity in the neural tube
702 (Supplementary Fig. 5 and [31]) as well as an enhancer cluster (EC) with validated
703 enhancer activity in zebrafish development (mint vertical highlight) [32]. The
704 schizophrenia-associated SNP rs1191551 (yellow vertical highlight) [57] and the distal
705 *FOXG1* TAD boundary (grey vertical highlight) also lie within the SRO. Abbreviations:
706 NPCCs, Neural Progenitor Cultured Cells. Differential UMI contacts between WT and
707 14q12-MRO-Del are represented as pink (positive log2FoldChange) and blue (negative
708 log2FoldChange) vertical highlights. ENCODE cCRE legend: Promoter-like signature
709 (red), Proximal (orange) and Distal (yellow) enhancer-like signature, DNAse H3K4me3
710 (pink) and CTCF-only (blue).
711
712 Figure 4: Evaluation of *FOXG1* CREs in the MRO. (A) A focus on the MRO region
713 showcases native *FOXG1* genomic interactions in WT that are lost in 14q12-MRO-Del.
714 Two active CREs (cyan highlights) from MPRAs in cerebral organoids and fetal brain
715 samples reside within the MRO.[33] Putative *FOXG1* CREs (cCRE1/2, purple highlights)
716 in the MRO are identified by the two H3K27Ac peaks conserved in HAP1s (ENCODE)
717 and neural cell types (RoadMap Epigenomic Project). (B) Dual luciferase assay in

HAP1s (human) and HT-22s (mouse) shows luciferase reporter expression is increased in the presence of cCRE1 and decreased in the presence of cCRE2 (n =4 for Empty, cCRE1 and cCRE2). Abbreviations: NPCCs, Neural Progenitor Cultured Cells. ENCODE cCRE legend: Distal enhancer-like signature (yellow), DNAse H3K4me3 (pink) and CTCF-only (blue).

Figure 5: Differential gene expression analysis in MRO and *FOXG1* loss. Volcano plot of DEGs in (A) 14q12-MRO-Del vs WT and (B) $FOXG1^{KO}$ vs WT highlighting down regulated (blue: log2FC<1) and upregulated (orange:log2FC>1) DEGs (adjusted p-value<0.05). Genes that overlap both MRO and FOXG1 loss datasets are indicated by triangles. (C) Heatmap of gene expression changes for overlapping DEGs between 14q12-MRO-Del, and $FOXG1^{KO}$ HAP1s. (n=3 for WT Clone A, WT Clone B, 14q12-MRO-Del and $FOXG1^{KO}$). Genes implicated in *FOXG1* pathophysiology and clinical phenotypes are highlighted (panels A and B) and appear in bold in panel C.

Figure 1: 14q12 microdeletions downstream of FOXG1 in this study.

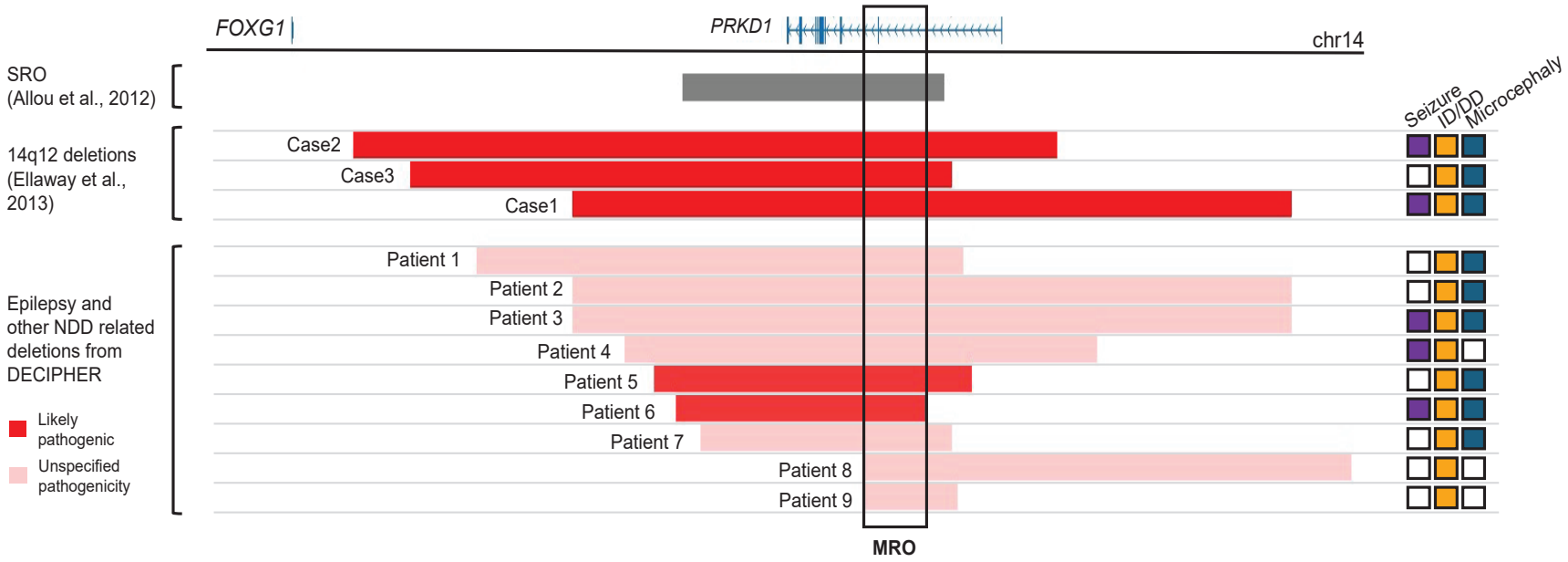

Figure 2 : FOXG1 expression is reduced with the loss of the MRO locus.

A. Relative fold change of *FOXG1* mRNA

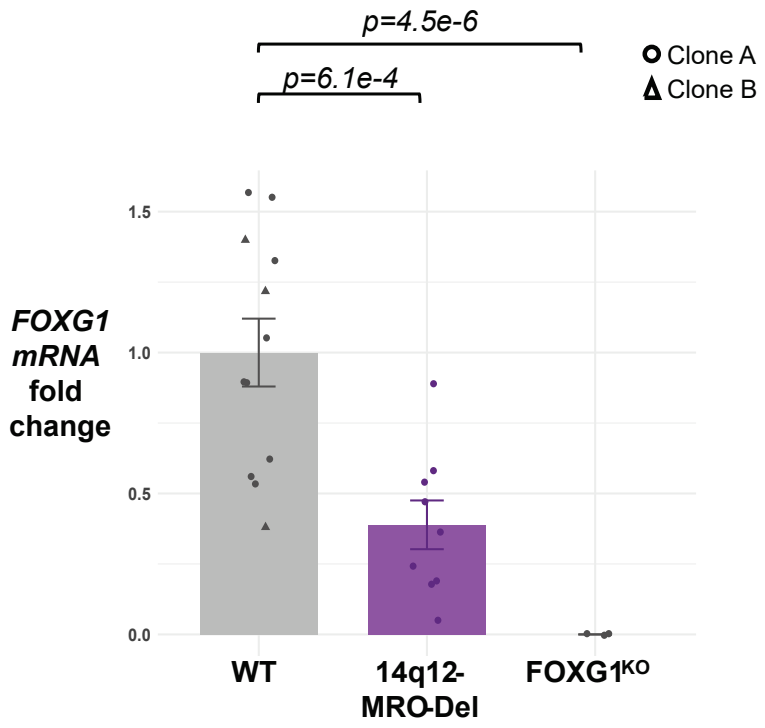

B. Relative fold change of FOXG1 protein

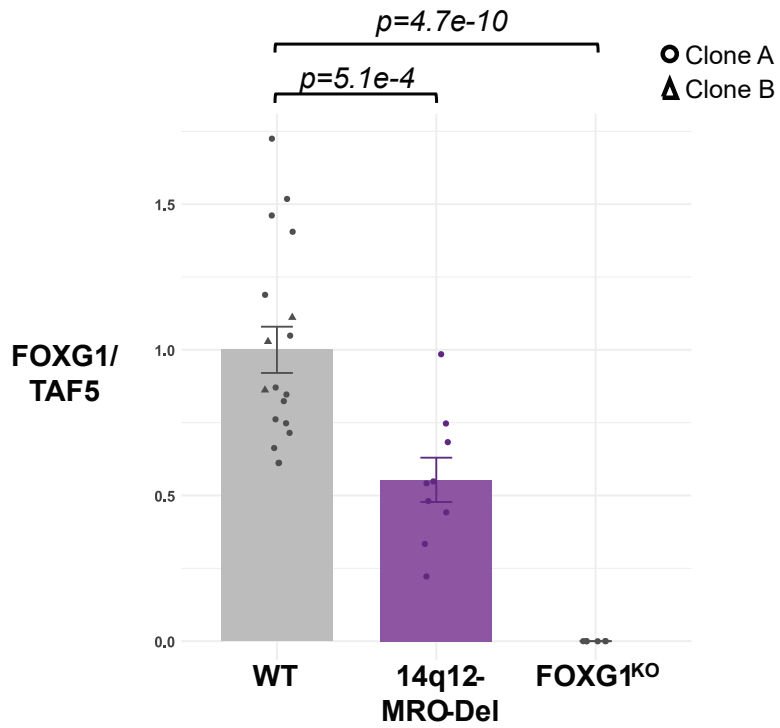

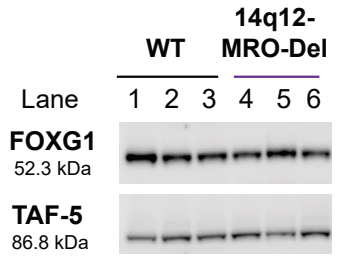

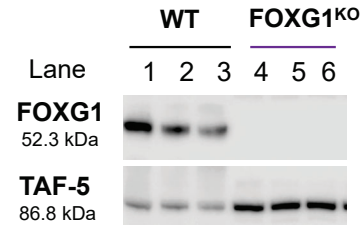

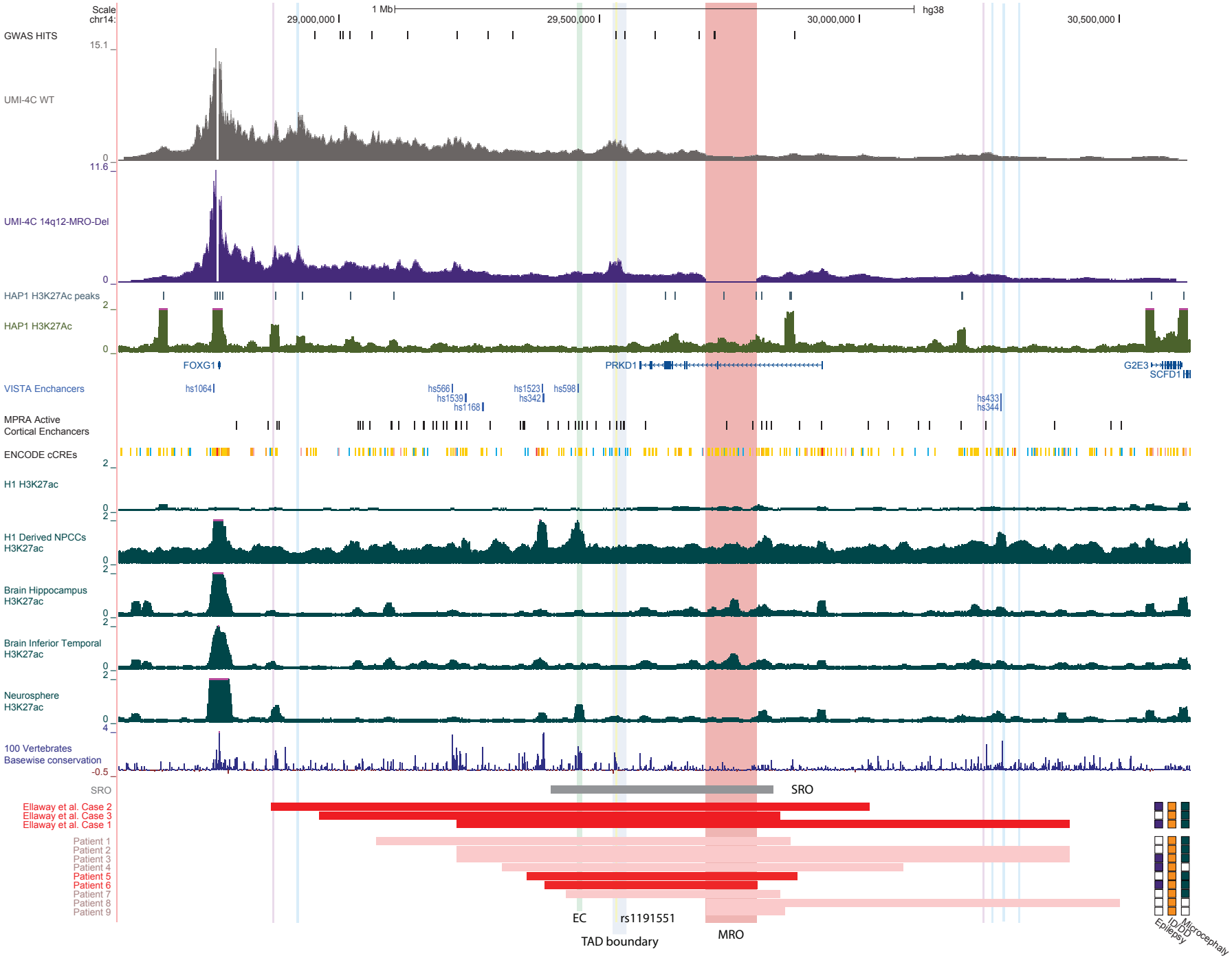

Figure 3: The FOXG1 regulatory region is a complex landscape of multiple known and putative CREs encompassing patient-specific deletions.

Figure 4: Evaluation of FOXG1 CREs in the MRO.

A

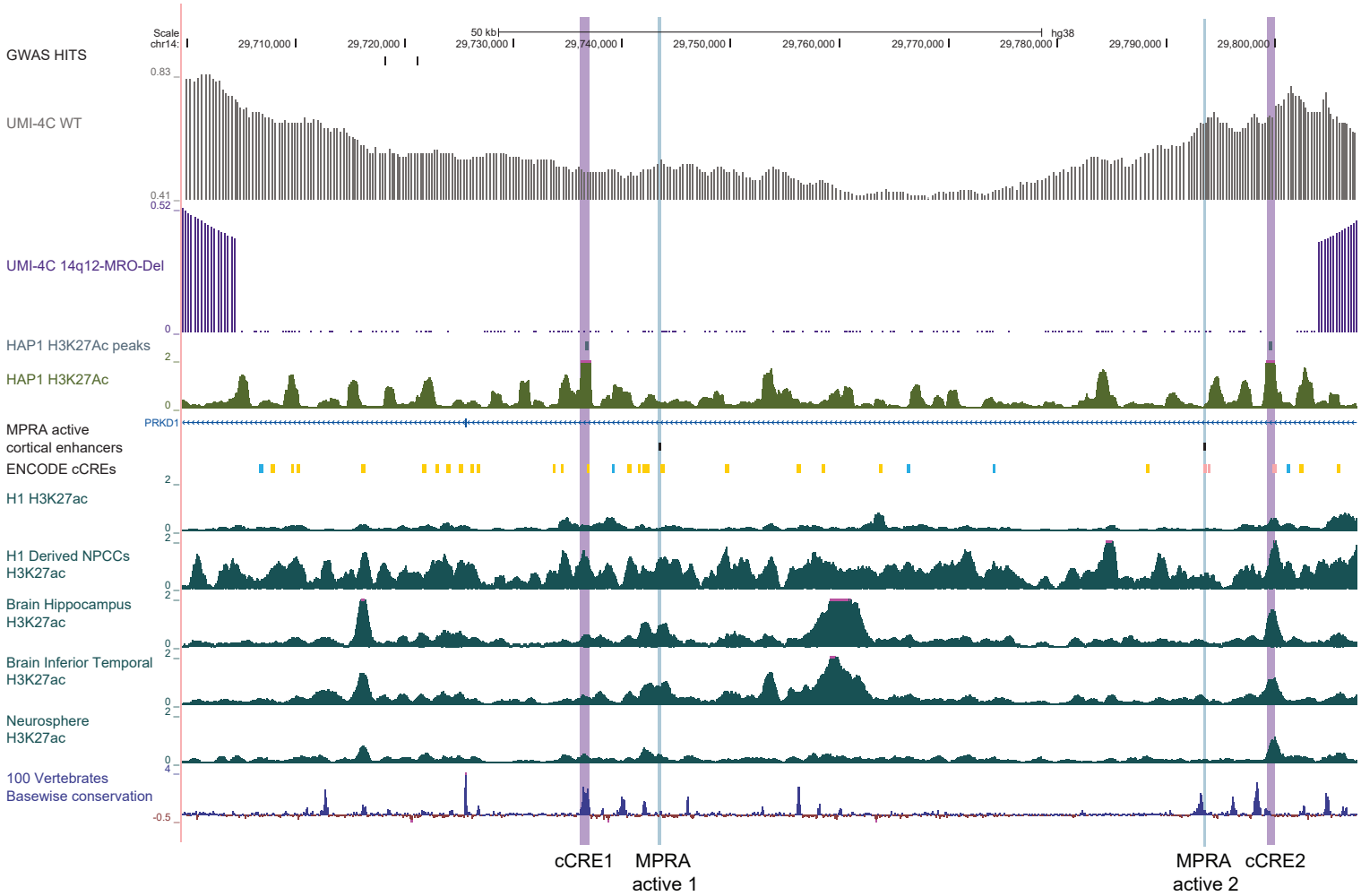

B **Relative fold change of luciferase reporter expression**

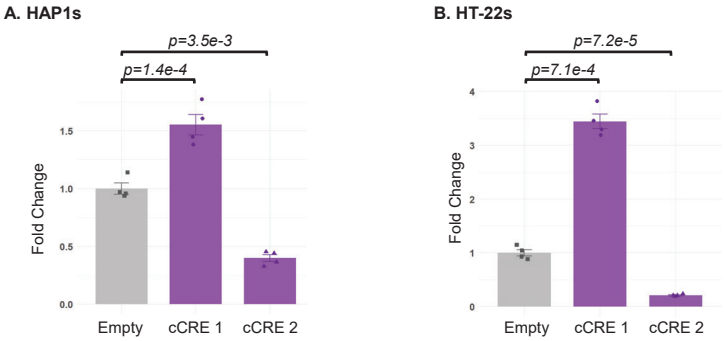
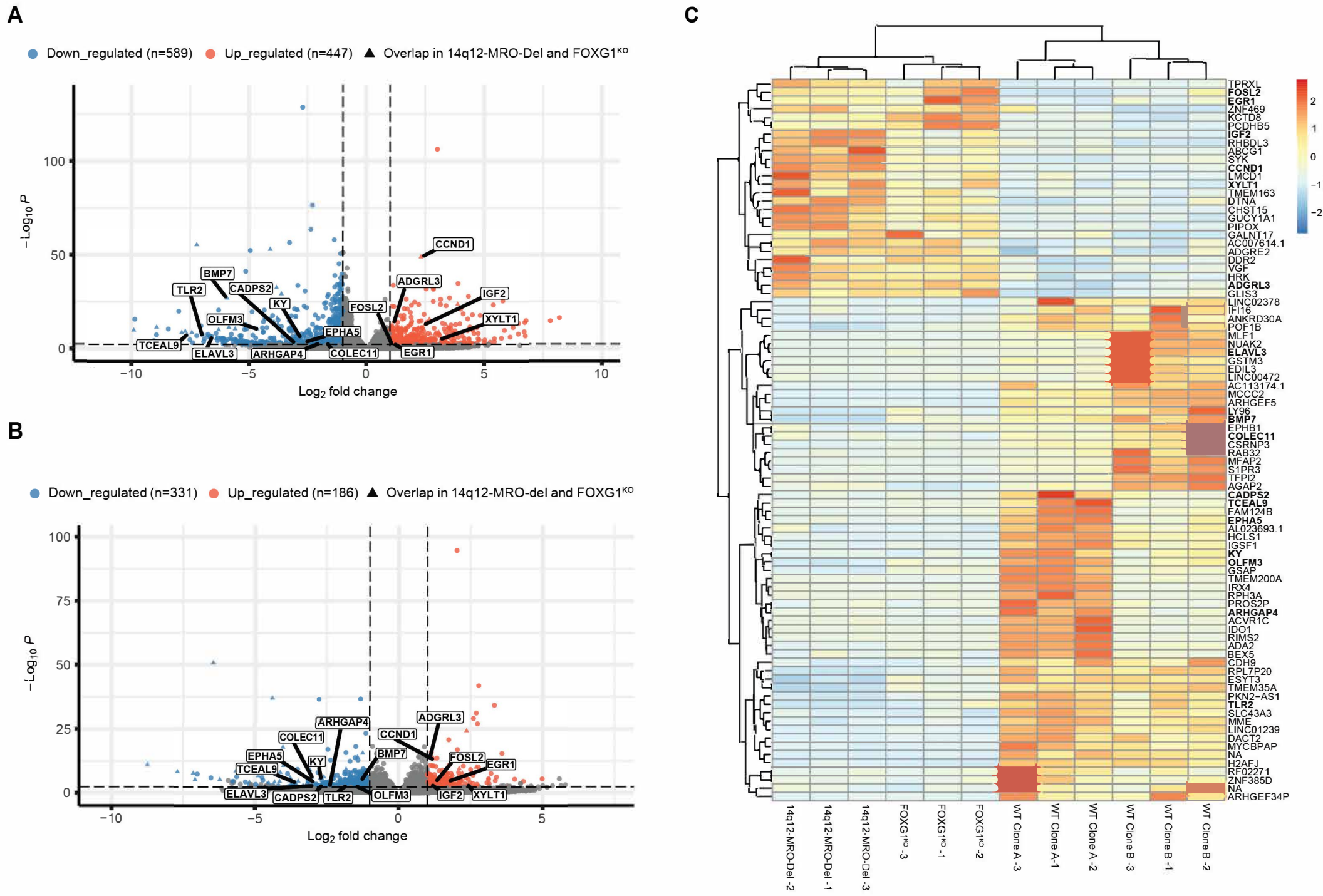
Figure 5: Differential gene expression analysis in MRO and FOXG1 loss.